

Analysis of Drop Bouncing On Solid Hydrophobic Surface

Praveen Kumar Sharma



भारतीय प्रौद्योगिकी संस्थान हैदराबाद
Indian Institute of Technology Hyderabad

Department of Mechanical & Aerospace Engineering

July 2015

Declaration

I declare that this written submission represents my ideas in my own words, and where ideas or words of others have been included, I have adequately cited and referenced the original sources. I also declare that I have adhered to all principles of academic honesty and integrity and have not misrepresented or fabricated or falsified any idea/data/fact/source in my submission. I understand that any violation of the above will be a cause for disciplinary action by the Institute and can also evoke penal action from the sources that have thus not been properly cited, or from whom proper permission has not been taken when needed.



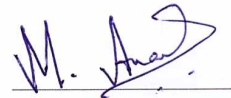
(Signature)

(Praveen Kumar Sharma)

(ME13M1032)

Approval Sheet

This Thesis entitled Analysis of Drop Bouncing On Solid Hydrophobic Surface by Praveen Kumar Sharma is approved for the degree of Master of Technology from IIT Hyderabad



(Dr. Anand Mohan) Examiner
Dept. of Chemical Engineering
IITH



(Dr. Raja Banerjee) Examiner
Dept. of Mechanical & Aerospace Engineering
IITH



(Dr. H N Dixit) Adviser
Dept. of Mechanical & Aerospace Engineering
IITH



(Dr. Chandrika Prakash Vyasrayani) Examiner
Dept. of Mechanical & Aerospace Engineering
IITH

Acknowledgements

I am grateful to my teacher who has taught me how to live a responsible life with his patience and love.

I would like to express my gratitude to my guide Dr. H N Dixit to allow me the freedom to work and at the same time to keep an eye to see that I do not get drifted from the main objective. I would especially like to thank him for his moral support and calmness, at the time when I have been running on low confidence with the thesis work. His honesty and humility, has always motivated us to work harder and has kept us grounded. And simultaneously, he has been the source of motivation for all our friends. Thus, the work environment, I have got to work has been vibrant and energetic.

I would also like to thank all my friends who have always maintained an atmosphere of co-operation and friendship. Thus, have made the thesis a joyful experience. I would like to thank my guide and the entire IIT Hyderabad system for providing us an excellent computational facility to work upon.

At last I would like thank my parents for their support and patience. I know, I have failed to be with them at various moments, they would have liked me to be with them. I would like to thank my younger brother for substituting for my role very nicely as far as possible.

Abstract

People are doing this problem from years because it has complex phenomenon such as contact line, spreading, splashing, re-bouncing to understand. Difficulty of problem increased by not having good contact angle models in numeric. Impact of drop on hydrophobic surface with static contact angle was studied using Gerris. "Volume of fraction" method is used to track the interface between two fluid in Gerris. Moto of this thesis to present numerical simulation work on drop bouncing, so our zone is hydrophobic substrate. Coefficient of restitution in problem shows the loss of energy in drop. Bouncing drop loses its kinetic energy and stretched to maximum radius at point kinetic energy equals zero, and surface tension effect act as spring in the system which store energy and force the drop to bounce back. Gravitational forces are less, and capillary wave form at the surface of drop. Capillary oscillation of the drop die due to viscosity present in drop fluid.

Contents

Declaration	ii
Approval Sheet	iii
Acknowledgements	iv
Abstract	v
1 Introduction	1
2 Numerical Equations and Multiphase model	3
2.1 Governing Equation	3
2.2 Non-Dimensional Numbers	4
2.3 Marker function Volume of fraction and equations	4
2.4 Volume of fraction method	6
2.4.1 Interface Normal vector Determination	7
2.4.2 Advection	8
3 Numerical Implementation and Validation	9
3.1 OpenFoam-2.3.0(OF) and Foam-extend-3.0(FE)	9
3.2 Gerris-1.3.2	10
3.3 Validation	11

4	Results and Dissussion	15
5	Appendix-1	21
6	Appendix-2	24
6.1	Geometric Mapping:The out of cell explicit linear mapping T^E	24
	References	28

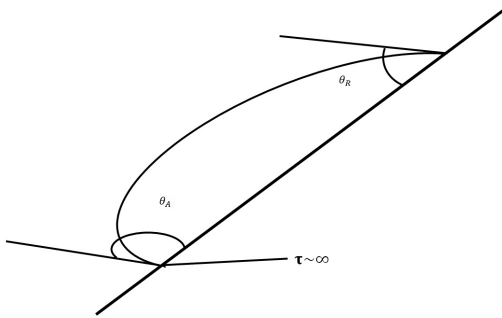
Chapter 1

Introduction

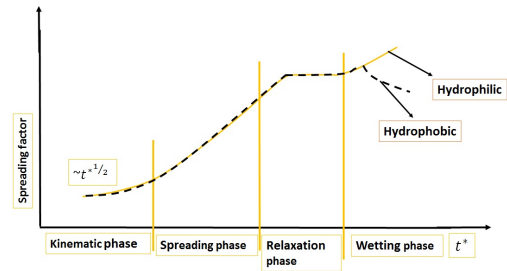
In this thesis I am presenting work on drop spreading in asymmetric domain. As experiments suggest that as we increase the lens power of camera to capture the fine detail, contact angle changes, in numeric also as we do grid refinement more and more, contact angle changes. By studying these phenomena some applications can improve such as spray cooling, ink-jet printing, spray printing, piezoelectric, in making of hydrophilic and hydrophobic surfaces and nano-generators which can convert mechanical energy into electric energy and many more. Several models based on conservation of energy that include drop initial potential energy, surface energy, final surface energy (changes due to deformation) and dissipation energy (to overcome viscous forces). Classification of numerical methods depend on work done by researchers in two groups. First one is finite element method on moving grid. Second one is based on fixed grid such as Cartesian grid. In fixed grid, first numerical solution to solve Navier-Stokes Eqn for fluid flow by Marker and Cell technique were done by [1]. Validity of their result only in initial stage of drop impact because in their method forces of liquid surface tension and viscosity were neglected and only in initial phase these forces are negligible. Alternative fixed grid front tracking methods are "Volume of fraction" (VOF) and Level set method. Vof algorithm which is used by [2] to solve Navier-Stokes eqn. Front tracking type method uses particle to track interface, VOF method track with geometrical interface reconstruction. In level-set modeling one can perform numerical computation involving curve and surfaces on a fixed Cartesian Grid. The level set method makes it very easy to follow shapes that change topology. The disadvantage of VOF method is the fact that it is difficult to compute accurate local curvature from volume fraction. So, Coupled Level-Set and Volume of Fraction "CLS-VOF" came into the picture. Its algorithm is developed by [3]. In CLS curvature is obtained via difference of level set function which derived from the level set function and VOF fraction at previous time step.

Phases in drop spreading is neatly explained by [4]. Based on that spreading is catego-

rized into four phases. First is Kinematic Phase. In which there is no ejection of spreading lamella. There is no effect of wettability, hence surface tension and viscosity in Kinematic phase. This phase is dependent on Reynolds number, if Reynolds number is large enough Kinematic phase is for good amount of time as explained in [4]. Second phase begins with lamella ejection due to shock wave known as spreading phase. Now, wettability comes into the picture, it also has an effect in drop spreading. As velocity and drop diameter increase, spreading rate becomes faster and as surface tension and viscosity increase, spreading rate decreases, vice-versa. Bond number and Weber number play their role in this phase. Third phase is relaxation phase. After spreading phase, drop may start recede or may splash, depending on Reynolds number, which is different for different combinations of substrate and fluid. For example, on a rough glass surface at high velocity of impact, splashing will happen.



(a) Dynamic Contact Angle.



(b) Phases of drop spreading explained in Rioboo.[4]

There are two types of surfaces: hydrophilic and hydrophobic. The classification of type of surface depends on the contact angle between substrate and fluid. If contact angle is less than 90° , substrate is hydrophilic and if contact angle is greater than 90° , substrate is hydrophobic for fluid. Motive of this thesis is to present numerical simulation work on drop bouncing, so our zone is hydrophobic. We took contact angle is 170° . Contact angle is divided into two types: dynamic contact angle and static contact angle. Dynamic contact at any moment is a function of Capillary number (which shows dependency on contact line velocity), and equilibrium contact angle θ_E .

Chapter 2

Numerical Equations and Multiphase model

2.1 Governing Equation

Let us consider the system of governing differential equations in vector form, describing the conservation of mass Eq. (2.1), momentum and energy Eq.(2.2) :

$$\nabla U = 0 \quad (2.1)$$

$$\rho(c) \left[\frac{\partial U}{\partial t} + U \cdot \nabla U \right] = -\nabla p + \rho(c)g + \mu [\nabla U + (\nabla U)^T] + f_{sv} \quad (2.2)$$

$$\rho(c) = \rho_1 C + \rho_2(1 - C) ; \mu(c) = \mu_1 C + \mu_2(1 - C) ; f_{sv} = \sigma k \hat{n} \delta$$

$$\frac{\partial C}{\partial t} + U \cdot \nabla C = 0 \quad (2.3)$$

U = velocity vector (u, v) ; t = time; \hat{n} = unit normal vector of interface ; f_{sv} = surface tension force per unit volume ; g = acceleration due to gravity ; P = pressure ; μ = viscosity of multiphase fluid; ρ = density of multi-phase fluid ; k = mean curvature of interface ; σ = surface tension co-efficient;

2.2 Non-Dimensional Numbers

When drop impact on surface drop spreading diameter, is function of density of fluid1 ρ_1 , density of fluid2 ρ_2 , initial diameter D , initial height h , gravity g , surface tension σ , dynamic viscosity of fluid1 μ_1 , dynamic viscosity of fluid2 $\mu_2 \sim 0$. The Buckingham π theorem is a key theorem in dimensional analysis as we know the number of non-dimensional(n)=number of variable(r)-number of fundamental dimensional (f). Where following are variable:

$$\rho = \frac{kg}{m^3} \quad D = m \quad h = m \quad g = \frac{m}{s^2} \quad \sigma = \frac{kg}{s^2} \quad \mu = \frac{kg}{m-s}$$

$$r = 7, f = 3 \text{ So, } n = 4$$

According to Buckingham π theorem there are three non-dimensional number required.those are Reynolds number (Re), Weber number (We),bond number (Bo) or Eotvos number(Eo) and Atwood number(At) their is one more non-dimensional number Capillary number (Ca) which are dependent on Re and We . Here Reynolds number is ratio of inertia force by viscous forces, Weber number is ratio of inertia force by surface tension force, bond number is ratio of gravitational force by surface tension, capillary number is ratio of viscous force by surface tension force. Independent non-dimensional number are define as follows:

$$Re = \frac{VD\rho_l}{\mu_l} ; We = \frac{V^2D\rho_l}{\sigma} ; Bo = \frac{D^2g\rho_l}{\sigma} ; At = \frac{\rho_1-\rho_2}{\rho_1+\rho_2}$$

Dependent non-dimensional number are define as follows:

$$Ca = \frac{V\mu_l}{\sigma} = \frac{We}{Re}$$

2.3 Marker function Volume of fraction and equations

VOF is a technique which used to track the interface, so it is called front tracking technique which solve Navier-Stokes equation on fixed graph, in our case grid is axisymmetric.

In two phase domain value of volume of fraction function $H_i(x)$ has value 0 and 1 and at the interface its value change from 0 to 1 for example if phase A has value of $H_i(x)$ 1 and phase B has value of $H_i(x)$ 0. For the cell having interface value is between 0 and 1.

As boundary evolves with time, the boundary between different fluids is tracked by marker points,than marker function defined by interface location.If x is location in 1D, $H_i(x)$ define as follows:

$$H_i(x) = \begin{cases} 1 & \text{if } x \text{ is in fluid } i \\ 0 & \text{if } x \text{ is in fluid } i \end{cases}$$

As we know that particle of each fluid not lose its identity after time evolution of interface also, or when shape of interface changes. That means their is no change in no. of fluid particle on fixed grid, i.e material derivative of VOF function is zero:

$$\frac{DH}{Dt} = \frac{\partial H}{\partial t} + u \frac{\partial H}{\partial x} + v \frac{\partial H}{\partial y} = 0 \quad (2.4)$$

To track interface we take average of VOF function in each cell known as color function(C), which have value 1 and 0 in cell, shown in Fig. 2.1. But if interface in any cell we have fractional value of C than we smooth the color function, which denote as "indicator function" with many technique.

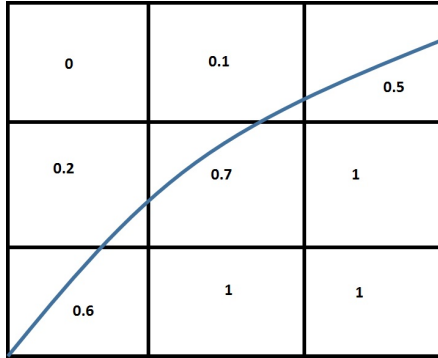


Figure 2.1: The interface line and the color function(C) value in each cell.

$$C_{i,j} = \frac{1}{\Delta x \Delta y} \int_v H(x,y) dx dy \quad (2.5)$$

$$I(x,y) = \int G(x-x', y-y') H(x,y) dx dy \quad (2.6)$$

I is directly construct from the interface, where G is smooth kernel. for advection of

color function We taken only 1D flow to explain VOF method, flow velocity in 1 direction is $u = U > 0$. Color function C is governed by equation following in which $F = UC$:

$$\frac{\partial C}{\partial t} + \frac{\partial F}{\partial x} = 0 \quad (2.7)$$

After discretization of above equation, value of C at time step n+1 in a cell.

$$C_j^{n+1} = C_j^n - \frac{1}{\Delta x} \int_t^{t+\Delta t} (F_{(j+\frac{1}{2})} - F_{(j-\frac{1}{2})}) dt \quad (2.8)$$

where $F_{(j+\frac{1}{2})} = UC_{(j+\frac{1}{2})}$ and $F_{(j-\frac{1}{2})} = UC_{(j-\frac{1}{2})}$

If we consider value of volume of fraction function constant in all over the domain. The value of C crosses the boundary is equal to value of cell in negative U direction of boundary, example if value of $C_{(i+\frac{1}{2})}$ is equals to C_i and value of $C_{(i-\frac{1}{2})}$ is equal to $C_{(i-1)}$. Then if We integrate equation(5), we get:

$$C_j^{n+1} = C_j^n - \frac{U\Delta t}{\Delta x} (c_j - c_{(j-\frac{1}{2})}) \quad (2.9)$$

By doing this results are not good, shown in book by [5] The reason of this is our assumption, i.e value of C is to represent the distribution of C in each cell by the cell average C_j . So, to solve this we need higher order function that recognizes that it is distributed over a cell.

2.4 Volume of fraction method

Following are the steps in VOF method:

- In step first, initial values of C used for construction of interface shape, PLIC is standard method is used for construction.
- In step second, advection of constructed interface in a given velocity field.
- In step third , reconstruction of interface shape.

In Standard reconstruction method PLIC, interface in each mixed cell is represented by a segment perpendicular to the local gradient, $m = -\Delta C$. If $\Delta x = \Delta y = h$ of a cell. If we integrate Eq.(2.4) over square cell (i,j) of side h of Cartesian 2-D grid and use $C_{i,j}$.

$$h^2 \frac{\partial_{i,j}(t)}{\partial t} + \int_{\Gamma} u \cdot r H(x, t) dl = 0 \quad (2.10)$$

Where Γ is cell boundary and r is outgoing normal vector, Integration of Eq. (2.10) gives following equation:

$$h^2 (C_{i,j}^{n+1} - C_{i,j}^n) = -(\phi_{x:(i+\frac{1}{2}),j}^n - \phi_{x:(i-\frac{1}{2}),j}^n) - (\phi_{i,y:(j+\frac{1}{2})}^n - \phi_{i,y:(j-\frac{1}{2})}^n) \quad (2.11)$$

Right hand side terms in equation 8 cancel-out, when sum over all the grid cell with appropriate boundary condition, internal fluxes cancel-out. So, Eq. (2.11) becomes:

$$\sum_{i,j} C_{i,j}^{n+1} = \sum_{i,j} C_{i,j}^n \quad (2.12)$$

2.4.1 Interface Normal vector Determination

There are number of methods for evaluation of normal vector, it can be based on finite difference approximation of volume of fraction gradient ΔC , to understand this let's take 3×3 block of cells having interface. Following are the methods to evaluate interface unit normal:

- Young's Finite-Difference Method
- Center-Columns Difference Method
- The Elvira Method
- The least-Square Fit Method

Determination of α

After calculation of normal vector m_i , α is determined by area convergence in 2D grid. Determination of area $A(\alpha)$ of polygon ABFGD and compare it with $C \Delta x \Delta y$, until the difference between the two is less than predefined tolerance. Calculation of Area of polygon ABFGD is given in Appendix-1.

2.4.2 Advection

Estimation of interface at next time step can be approximated by Geometric method or Fluxing methods. In Geometric method by advecting end points and in Fluxing method by computing the reference phase fluxes across the cell boundary. In 1D follow the interface as it advected by a discretized velocity field $u(x)$. In 2D : 1D advection in two direction are performed in sequence. To reduce possible asymmetries induced by the splitting. We consider first a motion along the x-direction than along the y-direction on odd time steps and vice-verse on even time steps. The consisting condition $0 \leq C \leq 1$ is satisfied after advection in each grid cell. Geometrical one-dimensional linear mapping method : In it two linear mapping. First is out-of-cell, in it we mark-out deformed cells in the original grid to update the volume fraction data. Second is onto-cell mapping we compute the area that will be advected into each grid cell. Both methods are discussed in Appendix-2.

Chapter 3

Numerical Implementation and Validation

OpenFoam-2.3.0(OF), Foam-extend-3.0(FE) and Gerris-1.3.2 are CFD codes used to simulate numeric work. In chronological order work starts from OF then FE and in the end switches to Gerris.

3.1 OpenFoam-2.3.0(OF) and Foam-extend-3.0(FE)

OpenFOAM (Open Field Operation and Manipulation) is primarily a C++ toolbox for the customization and extension of numerical solvers for continuum mechanics problems, including computational fluid dynamics (CFD). To simulate multi-phase problems OF has Volume of Fluid laminar solver InterFoam. There are two schemes for solving the Navier-Stokes equation, known as SIMPLE (Semi-Implicit Method for Pressure-Linked Equation) and PISO (pressure Implicit with Splitting of Operators). After each iteration of the SIMPLE multi-phase model equation will solve to update field variables. In the SIMPLE scheme is solved in the following four steps:

- Momentum Predictor : Solve the momentum equation to calculate the velocity field using best-guess initial values. Under-relaxation is normally used.
- Pressure Poisson: Use the predicted velocities to get information of pressure values.
- Calculate updated flux values for the cell faces.
- Calculate the new best-guess velocity field from the new set of face fluxes. Once the process has converged, this velocity field will satisfy both mass and momentum

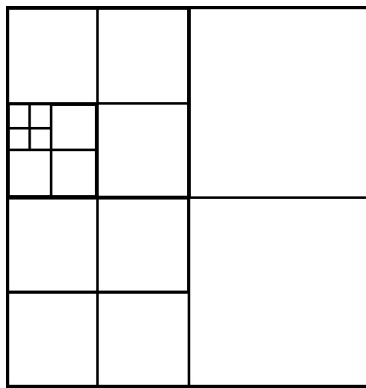
conservation.

While to use PISO scheme within time-step before PISO algorithm multiphase equation solved. Following is way to solve the PISO scheme:

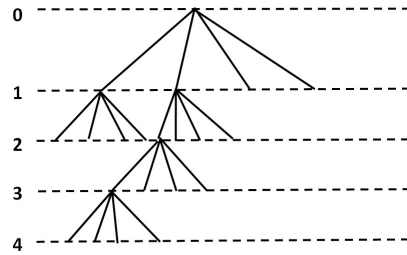
- Predictor: The momentum equations are optionally solved using a best-guess pressure field to produce a best-guess velocity field.
- Pressure Poisson: The best-guess velocities are used to solve the pressure equation.
- The velocity field is corrected using the new pressures.

3.2 Gerris-1.3.2

Gerris is developed by Stéphane Popinet[6]. It only work in cartesian coordinates. It is second order converge multiphase solver, which solve time dependent incompressible Euler Eqn's by adaptive mesh projection method. It discretize the domain by quadtree(in 2D) and octrees(in 3D) only for structured meshes. Quadtree discretization is shown in Fig. 3.1b, which clears how refinement happens to capture the interface. Adaptive mesh refinement works in Gerris according to specified Refinement level. For Example, if refinement level is n ratio of largest grid size to smallest grid size is $\left[\frac{X_l}{X_s} = 2^n\right]$ ($\Delta x = \Delta y = X$).



(a) Dynamic Contact Angle.



(b) Grid discretization in 2D by Quadtree[6].

3.3 Validation

Validation of Vof Model

To check the accuracy VOF of interfoam solver, we test the Hysing bubble rise [7]. This is simple test in which rise of bubble height has been done in 2D domain of mesh 64×128 , see Fig. 3.2. This test showed that VOF model in Open-Foam is not working well. As we can see the difference in shape and the rise of centroid height in Fig. 3.3 and Fig. 3.4. While FE and Gerris giving acceptable results of shape of bubble and centroid height rise with time.

ρ_1	ρ_2	μ_1	μ_2	g	σ	Re	Eo
1000	100	10	1	0.98	24.5	35	10

Table 3.1: Physical parameters and dimensionless numbers defined in the Hysing the test cases [7]

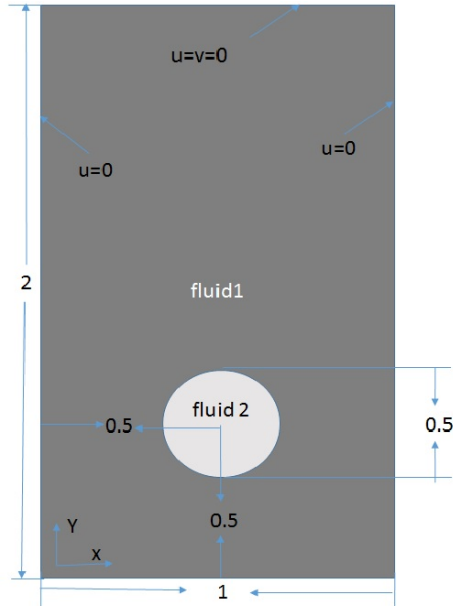


Figure 3.2: Hysing Test Domain [7].

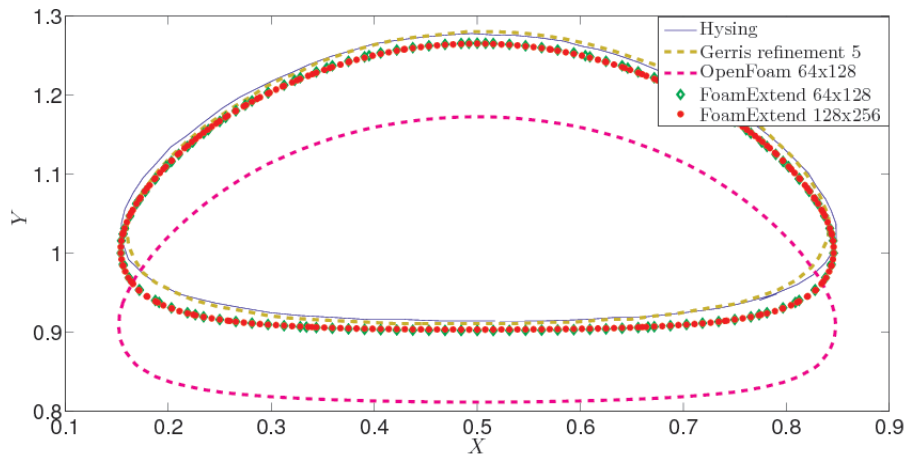


Figure 3.3: Bubble shape comparison OF, FE and Gerris with hysing at 3 sec.

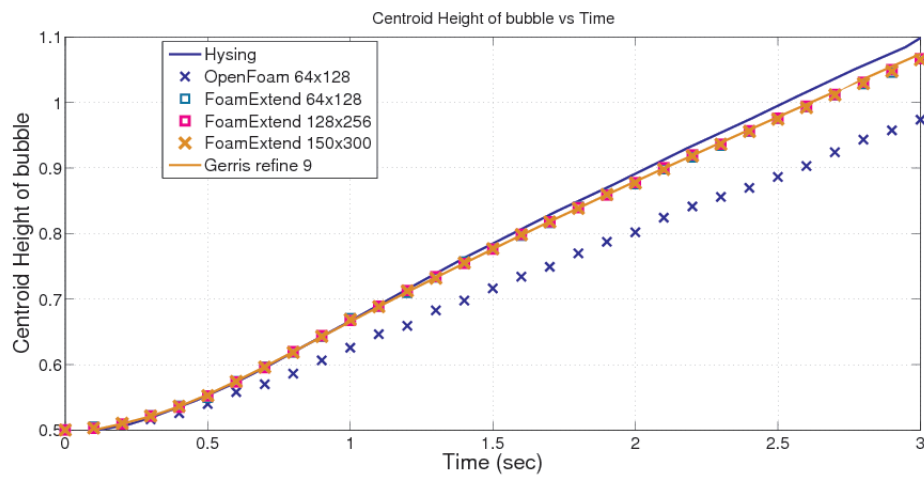


Figure 3.4: Height rise with time comparison of centroid for bubble rise for OF, FE, Gerris with hysing test case.

Contact Angle Model Validation

To know about the accuracy of contact angle model, we check with Rioboo's Experimental result[4] in axisymmetric domain having grid points 150×1100 . For $Re=1928$, $We=24$ and $Bo=0.58$, that means viscous and surface force effects are negligible. Numerical study for these non-dimensional number was done by both available contact model in OF i.s 'constantAlphaContactAngle' which is used for static contact angle θ_E and 'dynamicAlphaContactAngle' as name suggest it is for dynamic contact angle(advancing contact angle is θ_a and receding contact angle θ_r). The result comparison between OF numeric and experimental are shown in Fig. 3.5 for 'dynamicAlphaContactAngle'. Table 2 shows the parameter used for Rioboo et al experiment.

$D_0(mm)$	$v(m/s)$	σ	ρ_1	ρ_2	μ_1	μ_2	θ_E	θ_a	θ_r	Re	We	Bo
2.1	0.92	0.074	1000	1.225	10^{-3}	1.813×10^{-5}	7.744	10	6	1928	24	0.58

Table 3.2: Specification of Rioboo et al Experimental drop parameter [4]

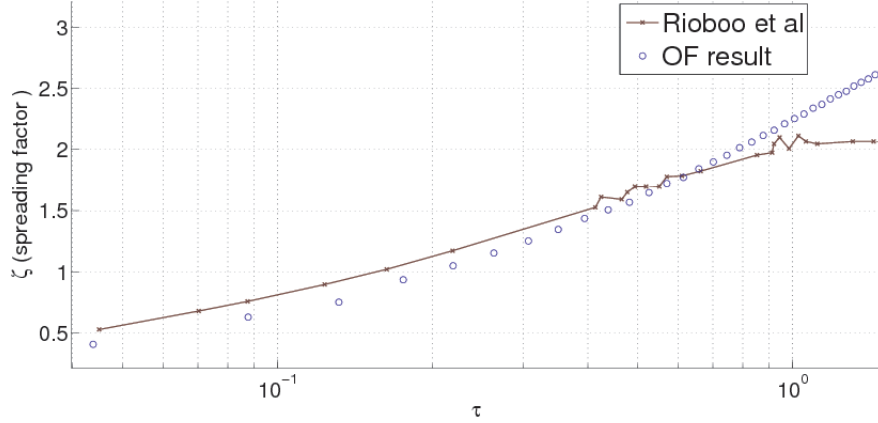


Figure 3.5: OF comparison with Rioboo Experiment having parameter Table 3.2.

In initial short period result is in range of acceptance, as seen in Fig. 3.5 because inertial effects are important, as we seen in kinematic phase. While as time increase viscous and surface force effect become important. When wettability comes into picture numerical results of OF starts deviates from experimental results. So, it can be conclude that OF dynamicAlphaContactAngle model is also not upto the mark. OF dynamicAlphaContactAngle model equation is:

$$\theta_d = \theta_E + (\theta_a - \theta_r) \times \tanh \left[\frac{V_c}{U_\theta} \right] \quad (22)$$

where θ_d is dynamic contact angle in OF which is function of θ_a and θ_r and velocity of contact line. This is an ad hoc model.

Chapter 4

Results and Dissussion

In this chapter we present the results of drop bouncing obtained using the multi-phase solver of Open-Source code discussed in previous chapter. The aim is to do axisymmetric study of drop impact on hydrophobic substrate. So that idea for scaling analysis can we produced to estimate the energy balance because coefficient of restitution occurs for bouncing drop.

Objective:

Drop of fluid1 having initial radius R release from initial height h , density ρ_l and dynamic viscosity μ_l while ρ_g μ_g are density and dynamic viscosity of fluid2. Non-dimensional numbers are same as taken by Richard, D and Quéré [8]. Table 4.1 gives information of the parameters value related to asymmetric domain shown in Fig. 4.1. As we seen in Fig. 4.2 Coefficient of Restitution ($\epsilon = |\frac{v_{i+1}}{v_i}|$) for bouncing drop is not equal to 1. The $\epsilon \geq 0.88$, which is also satisfy the experiment result of Richard and Quéré ϵ [8]. That means decay of available energy after drop impact happens.

$R(mm)$	h	σ	θ_c	ρ_l	ρ_g	μ_l	μ_g	Re	We	Bo
0.05	0.5	0.0007	170	1000	1.225	0.001	$1.84e^{-5}$	156.6	0.7	0.035

Table 4.1: Parameters for drop bouncing.

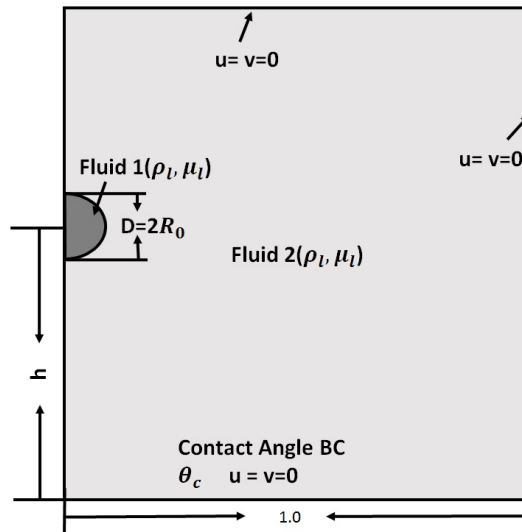


Figure 4.1: Domain for drop impact.

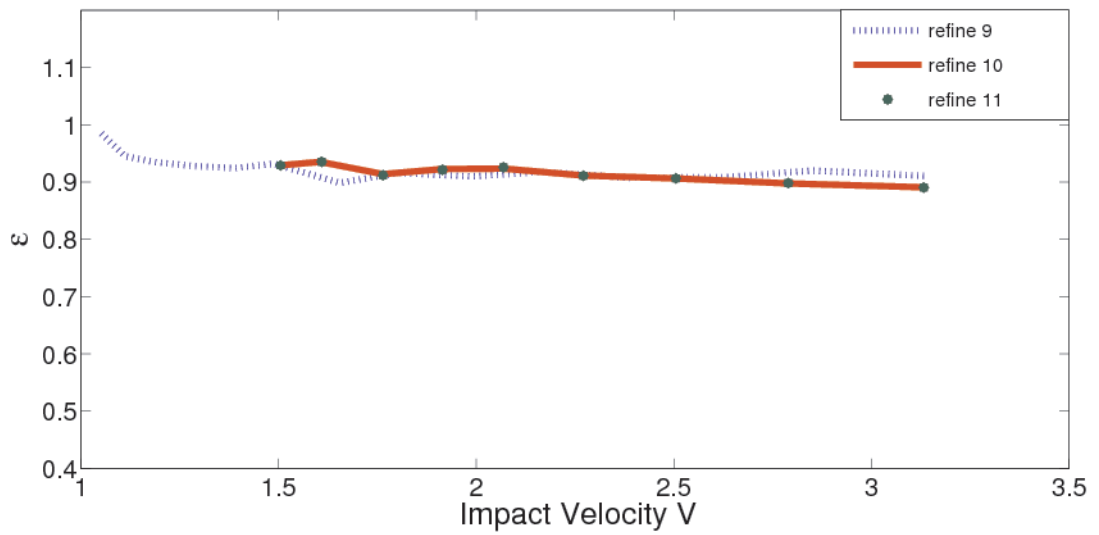


Figure 4.2: Coefficient of restitution vs velocity impact Table 4.1.

Effect of Grid Refinement

Fig. 4.3 shows the effect of grid refinement level in Gerris. Through this it can be suggested that there are two possible reasons for these differences. First is between refine 7 to refine 9, diffusion is dominant due to a coarse grid. As the number of grid points is enhanced, the smallest possible grid length decreases by the 2^2 factor, and the number of bounces increases by a large amount. While further increase in grid points and decrease in smallest grid length 2^2 , dissipation of energy at the contact line is increased relatively more than refine 9 because the contact angle boundary condition is grid dependent, as shown by Afkhami et al [9]. Due to which, the decrease in height of bounce after impact in further bounces is more than refine 9 but not much increase in the number of bounces.

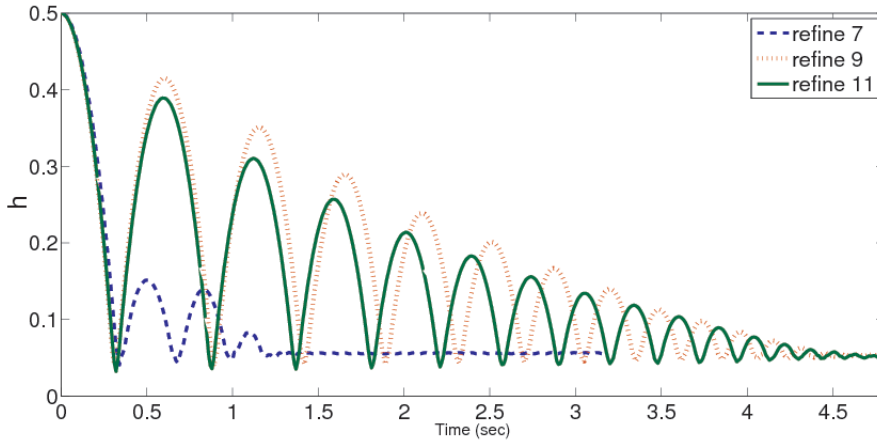


Figure 4.3: Effect of grid refinement in Gerris. Refine level 7, 9, 11 are presented here for parameters belong to Table 4.1.

Effect of Fluid2 viscosity

For same refinement level 9 in Gerris Fig. 4.4 shows the loss height due to fluid2 drag. For very small dynamic viscosity of fluid2 (viscosity in our case is $\mu 1e^{-20}$), fluid2 drag is so small it can be neglected. So, a part of initial energy goes into loss because of fluid2 dissipation.

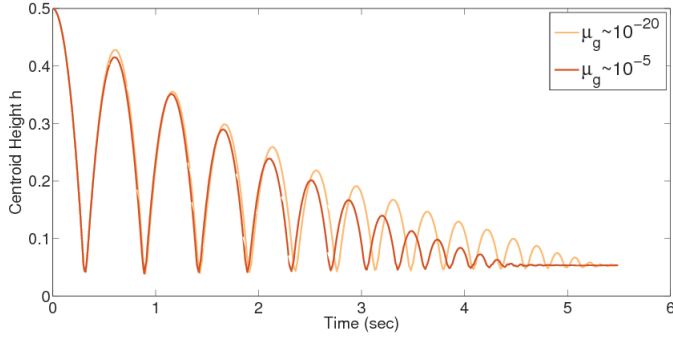


Figure 4.4: Loss in height of bounce due fluid drag for refine 9, Table 4.1.

Effect of Weber number

Fig. 4.6 shows the drop at maximum stretch on hydrophobic surface according to We . At maximum stretch radius increased to $R+x$, where R is initial radius of drop like a oblate spheroid shown in Fig. 4.5. Surface Area of spheroid:

$$S_{oblate} = 2\pi(R+x)^2 \left(1 + \frac{1-e^2}{e} \tanh^{-1}(e)\right) \quad (4.1)$$

where $e^2 = 1 - \frac{c^2}{(R+x)^2}$ c can be calculate by equal the volume of sphere and oblate spheroid
 $c = \frac{R^3}{(R+x)^3}$

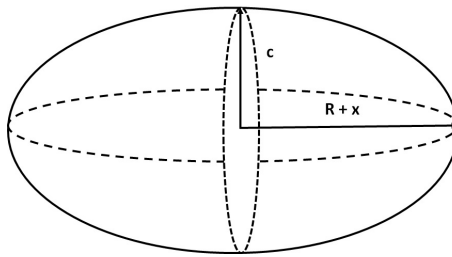


Figure 4.5: Oblate Spheroid shape of drop at maximum stretch.

So, the elastic energy at maximum stretch is $\frac{32\pi\sigma x^2}{5}$. Richard and Quéré [8] showed $x = \sqrt{(5We/48)} R$ analytically by energy balance. Energy balance between initial surface energy plus kinematic energy of drop to final surface energy. So, x is directly proportional to $We^{\frac{1}{2}}$ which is also valid by numeric done in our work presented in Fig. 4.7. Due to increase in We no. x also increases. Which further increase the surface energy of drop. So, when drop bouncing back capillary-wave oscillation (as Bo no. is small gravity have negligible effect in oscillation.) starts at the the surface of drop. Amplitude of oscillation depend on the initial maximum stretch of drop. Due to surface force effects drop try to shrink towards mean radius R . But like spring it does not stop at radius R and shrink up-to some radius $R-x$ and so on. Due to this capillary oscillation energy of drop dissipate.

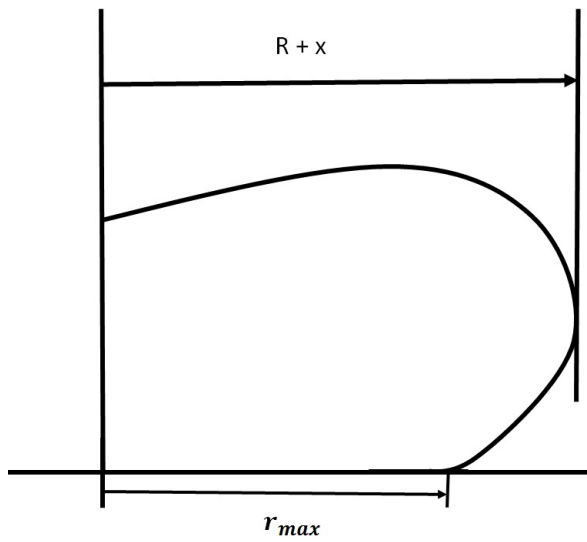


Figure 4.6: Symmetric diagram drop at maximum stretch.

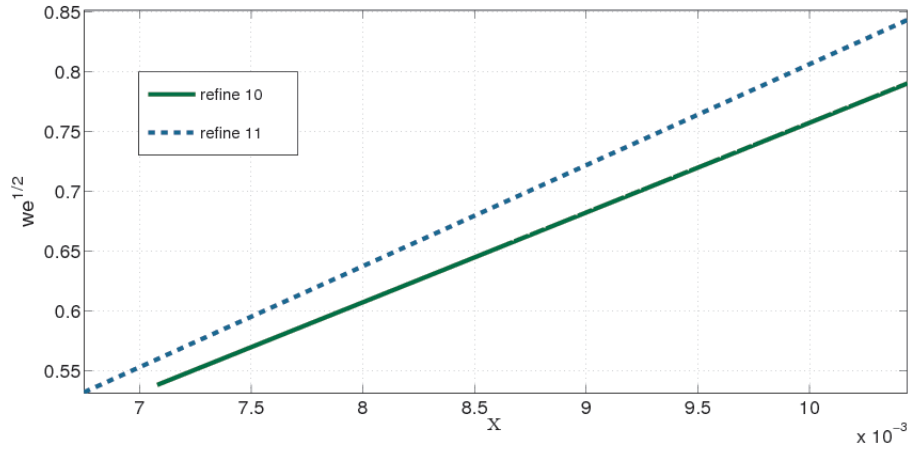


Figure 4.7: x variation with $We^{1/2}$.

Cause for lower coefficient of restitution than 1 can be consider in following points:

- Dissipation of energy at contact line, it is small because contact time is small.
- Fluid2 viscosity cause loss in kinematic energy of drop by viscous drag.
- Boundary layer Dissipation: energy dissipate at the time of impact due to viscous effect of fluid1. But it is also negligible because time of contact is very small.
- During rebound after impact capillary-oscillation present in drop causes maximum amount of energy loss.

Chapter 5

Appendix-1

In this Appendix we will see how we can calculate the value of area portion contain reference fluid. Fig. 5.1 is showing shaded area $A(\alpha)$ of reference fluid and area by color function is $C\Delta x\Delta y$ of same fluid. We need to find out zero of equation. $g(\alpha) = A(\alpha) - C\Delta x\Delta y$

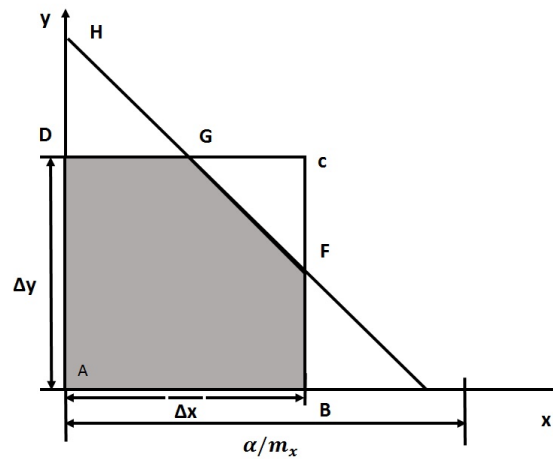


Figure 5.1: Shaded Area is need to calculate.

The area of ABFGD can be found by collecting counter-clockwise order the co-ordinates(x,y) of its vertices's

$$A = \frac{1}{2} \sum_{k=1}^n (x_k y_{k+1} - x_{k+1} y_k) \quad (5.1)$$

m_x, m_y are positive, so area of ABFGD in our case.

$$A = \frac{1}{2m_x m_y} [\alpha^2 - F_2(\alpha - m_x \Delta x) - F_2(\alpha - m_y \Delta y)] \quad (5.2)$$

where

$$F_2(z) = \begin{cases} z^2 & z > 0 \\ 0 & \text{otherwise} \end{cases}$$

Geometrically understanding of area in 2D of volume in 3D. Area is quadratic function of α , when interface line cut two consecutive cell side , then one of the two figure is triangle and it is linear when two intersection with the cell boundary are on opposite sides. Furthermore it is a continuous, strictly monotonically increasing function of α and it can be easily inverted.

Lets take 3D cell, than $m_x = m_1 x_1 + m_2 x_2 + m_3 x_3$ where m is pointing outside m_1 is positive. Volume of cell:

$$V = h^3 C = \frac{1}{6m_1 m_2 m_3} [\alpha^3 - \sum_{i=1}^3 F_3(\alpha - m_i h) + \sum_{i=1}^3 F_3(\alpha - \alpha_{max} m_i h)] \quad (5.3)$$

where $h = \Delta x = \Delta y$, $\alpha_{max} = \sum_{i=1}^3 m_i \delta x_i$,

Volume of tetrahedron under the $\Delta AEH = \frac{\alpha^3}{6m_1 m_2 m_3}$

Volume of ΔCEG and $\Delta BFH = \sum_{i=1}^3 F_3(\alpha - m_i h)$

Volume of $\Delta FDG = \sum_{i=1}^3 F_3(\alpha - \alpha_{max} m_i h)$

For 2D in area is consider in place of volume ,

$$A = h^3 C = \frac{1}{2m_1 m_2} [\alpha^2 - \sum_{i=1}^2 F_2(\alpha - m_i \Delta x_i)] \quad (5.4)$$

Chapter 6

Appendix-2

6.1 Geometric Mapping: The out of cell explicit linear mapping T^E

By linearized velocity field, interface at time t^n is mapped on interface at t^{n+1} . Equation of motion is $dx/dt=u(t)$ of particle $x(t)$ in velocity field $u(x)$. An explicit first-order scheme for its integration is

$$x(t^{n+1}) = x(t^n) + u[x(t^n)](t^{n+1} - t^n) \quad (6.1)$$

If we non-dimensionalize the space and time, x-component of velocity becomes CFL number. $x' = x/h; t' = t/\Delta t; u' = u\Delta t/h$ Using non-dimensional variables (primes are dropped).

$$x(t^{n+1}) = x(t^n) + u[x(t^n)] \quad (6.2)$$

Now we have cell (i,j). By linear-interpolation value of velocity at cell boundary marched into the cell linearly, As shown in figure. $u(x) = u_{i-\frac{1}{2},j}(1-x) + u_{i+\frac{1}{2},j}x$ coordinates at $x(t^{n+1})$:

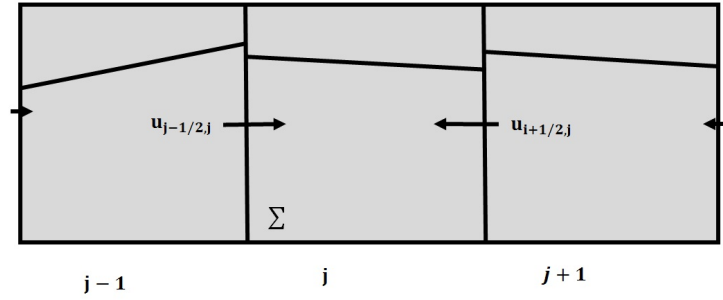


Figure 6.1: One-dimensional grid mapping T_x^E transforms the square cell Σ onto the rectangular $\Gamma_x[5]$.

$$x(t^{n+1}) = \begin{cases} bx + U_{i-\frac{1}{2},j} \\ y' = y \end{cases}$$

$b = 1 + U_{i+\frac{1}{2},j} - U_{i-\frac{1}{2},j}$ is contraction /expansion coefficient of out of cell linear mapping.

Geometric Mapping:The onto-cell implicit linear mapping T^I

Integrated equation of motion equation is following:

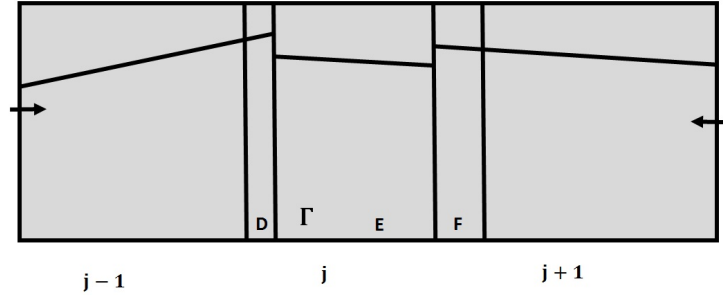


Figure 6.2: Three consecutive cells are transformed by the piecewise linear mapping T_x^E onto three rectangles which are projected back to the original grid [5].

$$x(t^{n+1}) = x(t^n) + u[x(t^{n+1})] \quad (6.3)$$

coordinates at $x(t^{n+1})$:

$$x(t^{n+1}) = \begin{cases} ax + aU_{i-\frac{1}{2},j} \\ y' = y \end{cases}$$

$a = 1/(1 + U_{i+\frac{1}{2},j} - U_{i-\frac{1}{2},j})$ is contraction /expansion coefficient of onto-cell linear mapping.

In explicit mapping, the whole computational domain is partitioned in a tessellation made up of pre-image rectangles such as γ_x . This ensure that no area is lost or fluxed twice. However the sequence of two consecutive onto-cell implicit mapping in the x and y direction does not conserve area.

Geometric Mapping: Combined Linear mapping

It is combination of out of cell explicit method and onto cell implicit method. The mapping sequence of in combined linear mapping method is T_x^I and T_y^E i.e transformation in x direction by implicit method and in y direction by explicit method to conserve area /mass exactly. to minimize asymmetries the combined mapping $T_y^E T_x^I$ at one time step should be alternated with $T_x^E T_y^I$ at next time step. For first transformation T_y^E coordinates of interface evolve in y- direction

$$\begin{cases} x' = x \\ y' = by + v_{i,j-\frac{1}{2}} \end{cases}$$

For second transformation T_x^I coordinates of interface evolve in x- direction

$$\begin{cases} x' = ax + aU_{i-\frac{1}{2},j} \\ y' = y \end{cases}$$

where b and a are contraction or expansion coefficient $b = 1 + U_{i+\frac{1}{2},j} - U_{i-\frac{1}{2},j}$ and $a = 1/(1 + U_{i+\frac{1}{2},j} - U_{i-\frac{1}{2},j})$

References

- [1] F. H. Harlow and J. P. Shannon. The splash of a liquid drop. *Journal of Applied Physics* 38, (1967) 3855–3866.
- [2] M. Pasandideh-Fard, Y. Qiao, S. Chandra, and J. Mostaghimi. Capillary effects during droplet impact on a solid surface. *Physics of Fluids (1994-present)* 8, (1996) 650–659.
- [3] M. Sussman and E. G. Puckett. A coupled level set and volume-of-fluid method for computing 3D and axisymmetric incompressible two-phase flows. *Journal of Computational Physics* 162, (2000) 301–337.
- [4] R. Rioboo, M. Marengo, and C. Tropea. Time evolution of liquid drop impact onto solid, dry surfaces. *Experiments in Fluids* 33, (2002) 112–124.
- [5] G. Tryggvason, R. Scardovelli, and S. Zaleski. Direct numerical simulations of gas–liquid multiphase flows. Cambridge University Press, 2011.
- [6] S. Popinet. Gerris: a tree-based adaptive solver for the incompressible Euler equations in complex geometries. *Journal of Computational Physics* 190, (2003) 572–600.
- [7] S. Hysing, S. Turek, D. Kuzmin, N. Parolini, E. Burman, S. Ganesan, and L. Tobiska. Quantitative benchmark computations of two-dimensional bubble dynamics. *International Journal for Numerical Methods in Fluids* 60, (2009) 1259–1288.
- [8] D. Richard and D. Quéré. Bouncing water drops. *EPL (Europhysics Letters)* 50, (2000) 769.
- [9] S. Afkhami, S. Zaleski, and M. Bussmann. A mesh-dependent model for applying dynamic contact angles to VOF simulations. *Journal of Computational Physics* 228, (2009) 5370–5389.